Nuclear Instruments and Methods in Physics Research A 787 (2015) 134–139

Contents lists available at ScienceDirect

Nuclear Instruments and Methods in Physics Research A

journal homepage: www.elsevier.com/locate/nima

Performances of photodiode detectors for top and bottom counting detectors of ISS-CREAM experiment

H.J. Hyun [a,1], T. Anderson [b], D. Angelaszek [c], S.J. Baek [d], M. Copley [c], S. Coutu [b], J.H. Han [c], H.G. Huh [c], Y.S. Hwang [a], S. Im [b], H.B. Jeon [a], D.H. Kah [a,2], K.H. Kang [a], H.J. Kim [a], K.C. Kim [c], K. Kwashnak [c], J. Lee [d], M.H. Lee [c,3], J.T. Link [e,f], L. Lutz [c], J.W. Mitchell [e], S. Nutter [g], O. Ofoha [c], H. Park [a,*], I.H. Park [d], J.M. Park [a], P. Patterson [c], E.S. Seo [c], J. Wu [c], Y.S. Yoon [c,3]

[a] Kyungpook National University, Daegu 702-701, South Korea
[b] Pennsylvania State University, University Park, PA 16802, USA
[c] University of Maryland, College Park, MD 20740, USA
[d] Sungkyunkwan University, Suwon 440-746, South Korea
[e] NASA GSFC, Greenbelt, MD 20771, USA
[f] CRESST(USRA), Columbia, MD 21044, USA
[g] Northern Kentucky University, Highland Heights, KY 41099, USA

ARTICLE INFO

Available online 26 November 2014

Keywords:
Cosmic ray
ISS-CREAM
Photodiode
Plastic scintillator
Thermal-vacuum
Vibration

ABSTRACT

The Cosmic Ray Energetics and Mass (CREAM) experiment at the International Space Station (ISS) aims to elucidate the source and acceleration mechanisms of high-energy cosmic rays by measuring the energy spectra from protons to iron. The instrument is planned for launch in 2015 at the ISS, and it comprises a silicon charge detector, a carbon target, top and bottom counting detectors, a calorimeter, and a boronated scintillator detector. The top and bottom counting detectors are developed for separating the electrons from the protons, and each of them comprises a plastic scintillator and a 20×20 silicon photodiode array. Each photodiode is 2.3 cm $\times$ 2.3 cm in size and exhibits good electrical characteristics. The leakage current is measured to be less than 20 nA/cm^2 at an operating voltage. The signal-to-noise ratio is measured to be better than 70 using commercial electronics, and the radiation hardness is tested using a proton beam. A signal from the photodiode is amplified by VLSI (very-large-scale integration) charge amp/hold circuits, the VA-TA viking chip. Environmental tests are performed using whole assembled photodiode detectors of a flight version. Herein, we present the characteristics of the developed photodiode along with the results of the environmental tests.

1. Introduction

After the discovery of cosmic rays [1], measurements of the energy spectrum, composition, and elemental abundances have been conducted in many experiments [2]. The energy spectrum can be described by the power law with respect to the energy E : $dN/dE \propto E^{-\gamma}$, where γ is the spectral index. There are energy regions not following this power law, known as the "knee" (between 10^{15} and 10^{16} eV) and "ankle" (around $10^{18.5}$ eV) [3]. The energy of the knee region can be considered as the maximum energy that most cosmic acceleration in the galaxy has reached. The measurement of a cosmic ray's composition is very important for understanding the knee and can yield information about the source and propagation mechanisms of high-energy cosmic rays. The Cosmic Ray Energetics and Mass in the International Space Station (ISS-CREAM) [4] experiment is planned for launch at the ISS in February 2015, aiming to measure the energy spectral features from 10^{12} eV to $\sim 10^{16}$ eV and the composition that might be related to the supernova acceleration limit [5]. The ISS-CREAM instrument shown in Fig. 1 comprises a silicon charge detector (SCD) for identifying incident cosmic rays, a carbon target, a sampling tungsten/scintillator calorimeter for the energy measurement of all nuclei, a segmented top and bottom counting detectors (T/BCD) for the electron/proton (e/p) separation, and a boronated scintillator detector (BSD) for additional e/p separation

* Corresponding author.
E-mail address: sunshine@knu.ac.kr (H. Park).
[1] Presently at Pohang Accelerator Laboratory, Jigokro-127-beongil, Nam-gu, Pohang 790-834, South Korea.
[2] Presently at Agency for Defense Development, Bugyuseong-daero, Yuseong-gu, Daejeon 305-152, South Korea.
[3] Presently at Institute for Basic Science, Yuseong-daero 1689-gil, Yuseong-gu, Daejeon 305-811, South Korea.

http://dx.doi.org/10.1016/j.nima.2014.11.075
0168-9002/

and detecting neutron signals. We develop large-area photodiode (PD) detectors for the T/BCD that measure the shower profiles of incoming particles, which helps to separate the electrons from the protons. In this paper, we report the performances of the developed silicon PD and measurement results of environmental tests for the T/BCD.

2. Top and bottom counting detectors

The T/BCD are designed to measure the scintillation light produced by a plastic scintillator when particles pass through the scintillator and the PD converts the scintillation light to an electric current. The PDs, coupled with the plastic scintillators, are operated at the full depletion voltage. Therefore, they detect not only the scintillation light but also incoming charged particles traversing them. The goals and performance requirements of the T/BCD are as follows:

- Separate electrons from protons for study of electron and γ-ray physics [6] by using the difference between electromagnetic and hadronic showers → Proton rejection factor is better than 1000 with 60% efficiency for 600 GeV electron
- Provide redundant trigger to the calorimeter and trigger for the minimum ionizing particle (MIP) for purpose of calibration → redundant trigger capability and MIP identification with signal-to-noise ratio (SNR) better than 5.

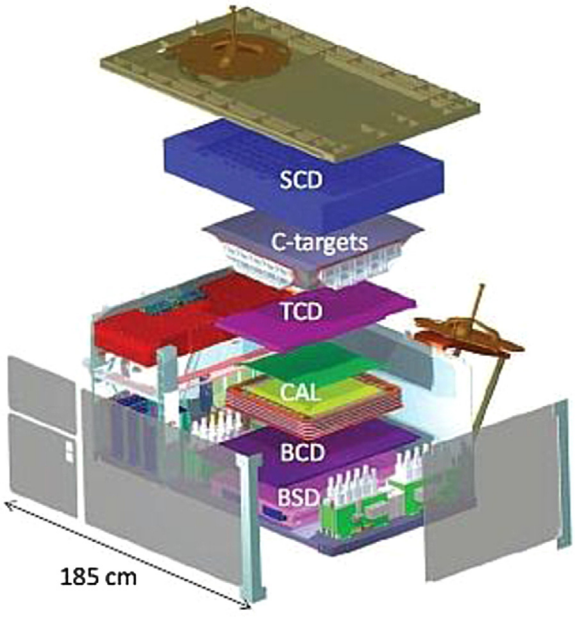

Fig. 1. Schematic of the cosmic ray energetics and mass instrument at the international space station.

The TCD is located between the carbon target and the calorimeter, and the BCD is located below the calorimeter. The energy information from the segmented PDs in this configuration allows distinguishing the electrons from the protons. The PD signals are amplified by VLSI (very-large-scale integration) charge amplifier and hold circuits, which the VA-TA Viking chips from IDEAS [7] are used for the front-end readout electronics.

The TCD and BCD comprise $500 \times 500 \times 5\ mm^3$ and $600 \times 600 \times 10\ mm^3$ plastic scintillators (EJ-200 from ELJEN Technology [8]), respectively. The emission wavelength range of the EJ-200 is 400 to 500 nm. The light produced in each detector is measured by a 20×20 PD array. The dimensions and design specifications are summarized in Table 1.

3. Silicon photodiode

3.1. Design and fabrication

The PD is manufactured on an n-type silicon wafer with a 6-in. diameter, 650 μm-thick, high resistivity ($>5\ k\Omega\ cm$), and ⟨100⟩−orientation. Various test patterns including $1.0 \times 1.0\ cm^2$ PDs and PD pixel arrays, and 18 PDs are designed on the wafer. The fabrication employs the conventional double-sided planar process [9] and is performed at the Electronics and Telecommunications Research Institute (ETRI) [10]. The junction side of the PD is formed by boron implantation into the bare wafer. The light entrance window on the ohmic side comprises an n^+ ion implanted layer and an anti-reflective coating (ARC) surface. The layers are optimized to provide a sufficient depletion depth and to acquire all of the incident light [11]. An n-channel stop structure [12] is employed as a field shaper to suppress the leakage current from the edge. The size of the PD is $2.3 \times 2.3\ cm^2$, and its active area is $2.0 \times 2.0\ cm^2$. Fig. 2 shows both sides of the fabricated silicon wafer.

3.2. Performances

The PDs are characterized by the leakage current and the bulk capacitance as functions of the reverse bias voltage at room temperature. The leakage current and the capacitance are measured using a Keithley 6517 picoammeter and HP 4266A LCZ meter, respectively. The full depletion voltage is determined to be 150–180 V from the capacitance measurement, and the operating voltage is determined to be 200 V. The PDs are classified depending on the leakage current value at the operating voltage. When the leakage current is less than $100\ nA/cm^2$ and there is no breakdown, the PD is classified as the good sensor. The leakage current levels of all PDs used for assembly are below $20\ nA/cm^2$ at the operating voltage.

The photosensitivity of the PD for the wavelength range of 350–1100 nm is measured at the Korea Research Institute of Standards and Science (KRISS) [13]. The measurement results for

Table 1
Specification of the top and bottom counting detectors.

Item	TCD	BCD
Dimensions (mm^3)	$901 \times 551 \times 30$	$951 \times 651 \times 33$
Weight (kg)	<13	<16
Thickness of plastic scintillator (mm)	5	10
Area covered by PDs (mm^2)	500×500	600×600
Number of PDs	400	400
Power consumption	<20 W for each detector	
First resonant frequency	>100 Hz	
Margin of safety (MS)	Positive value calculated using stress values from simulation	

the spectral responsibility and converted quantum efficiency are shown in Fig. 3. The black lines in Fig. 3 correspond to the PDs of the T/BCD, and the gray band indicates the wavelength range of the plastic scintillator. The quantum efficiency for the light from the plastic scintillator is measured to be 60–85%.

The SNR of the PD is measured using a ^{90}Sr radioactive source. A schematic diagram of the measurement is shown in Fig. 4; a coincidence trigger is used to select the signal events. The pedestal and signal distributions are shown in Fig. 5, and the SNR is measured to be 111 using commercial electronics. The SNR is measured with the same setup to be 71.2 for cosmic ray muons. The difference in the SNR between the radioactive source and muons is due to the noise, which depends on the data acquisition time.

The radiation hardness of the PD is tested with a 45-MeV proton beam at the Korea Institute of Radiological and Medical Sciences (KIRAMS) [14]. The PD is exposed to 1.18×10^{11} protons/cm^2, which corresponds to >5000 rad required by the ISS-CREAM experiment. The leakage current is increased up to $\sim$50 nA/cm^2, but the quality of the PD is not changed in our criteria for the good sensor [15].

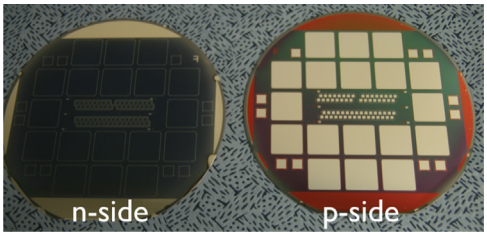

Fig. 2. Photographs of the photodiodes on a 6-in. and 650-μm-thick silicon wafer.

4. Environmental tests

The thermal-vacuum and vibration environmental tests are performed with the flight version of the T/BCD at the Korea Aerospace Research Institute (KARI) [16] and the Center for Automotive Mechatronics Parts at Keimyung University [17], respectively.

4.1. Thermal-vacuum test

In the thermal-vacuum test, the hot survival (operational) and cold survival (operational) temperatures are defined as $+55\,^{\circ}$C ($+40\,^{\circ}$C) and $-40\,^{\circ}$C ($-20\,^{\circ}$C), respectively. Four thermal cycles between the hot and cold operational temperatures are performed while keeping the chamber pressure less than 10^{-5} Torr. The experimental setup and test procedures depending on the thermal cycle are shown in Figs. 6 and 7, respectively. The T/BCD are put into the chamber of 1 m in diameter, and four thermocouples are attached to each detector. The connections between the detectors and control electronics are accomplished by feedthrough port plates placed on both sides of the chamber. When the chamber is at a vacuum and the temperature is stabilized, the first thermal cycle begins. The temperatures are monitored continuously during the test. The gray region in Fig. 7 indicates the survival temperatures; the detectors are unpowered in this cycle. Except for this region, the functional tests, e.g., pedestal and calibration runs, are performed at every plateau, and the power-cycled test is

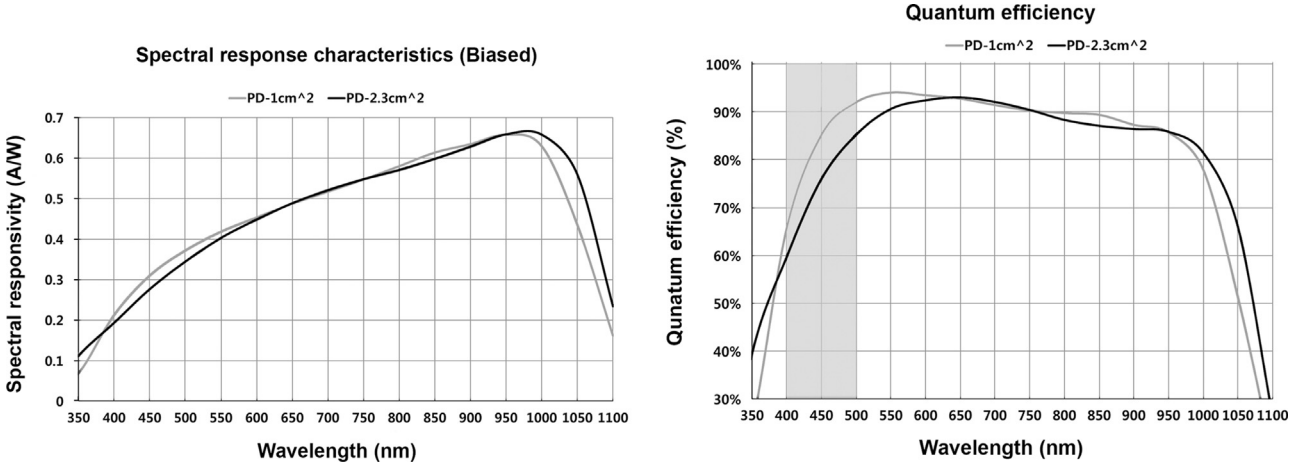

Fig. 3. Spectral responsibility (left) and quantum efficiency (right) as functions of wavelength. Grey band represents wavelength range of plastic scintillator.

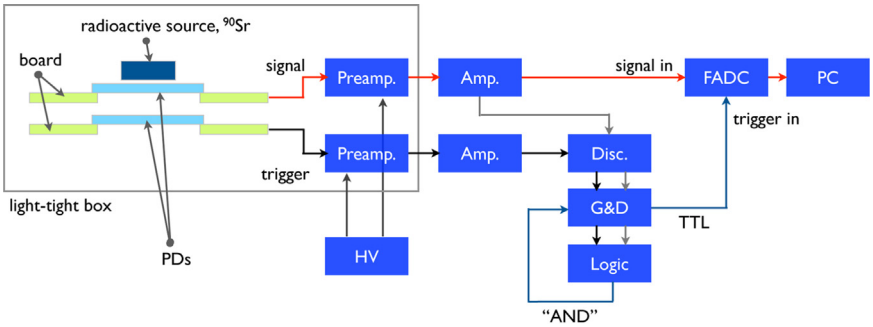

Fig. 4. Schematic of experiment setup for signal-to-noise ratio measurement using ^{90}Sr radioactive source.

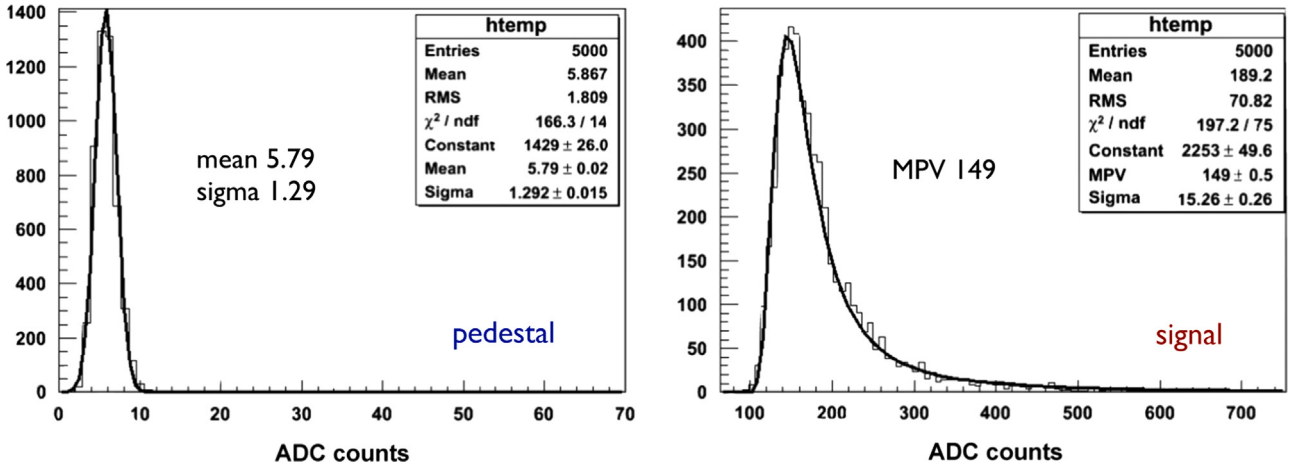

Fig. 5. Pedestal and signal distributions obtained using ^{90}Sr radioactive source.

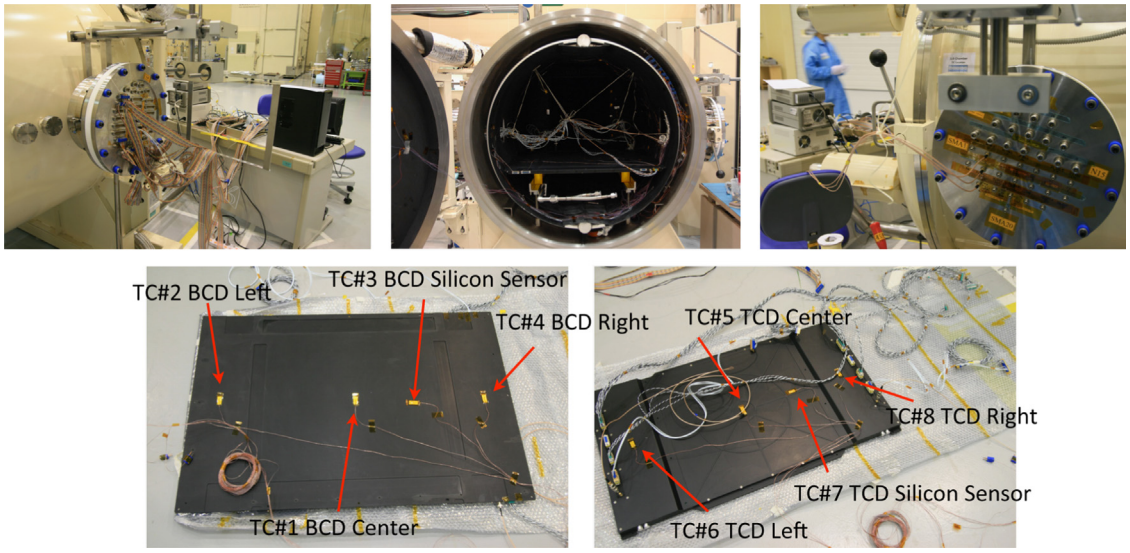

Fig. 6. Experimental setup for thermal-vacuum test.

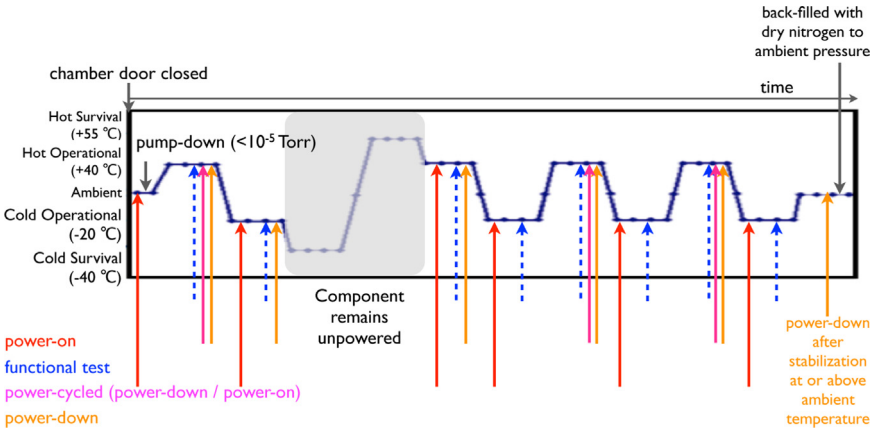

Fig. 7. Procedure for thermal-vacuum test.

performed at the plateau of every hot operational temperature. The chamber is heated toward the ambient temperature after all of the thermal cycles. Once the detectors completely stabilize at or above the ambient temperature, the detector power is turned off and the chamber is back-filled with dry nitrogen to the ambient pressure. The T/BCD are normally operated with a slightly increased noise level during the test. The power is not turned on at the low temperature, because of a glitch in one of the control signals. This problem is solved by adding a capacitor to the line after the test.

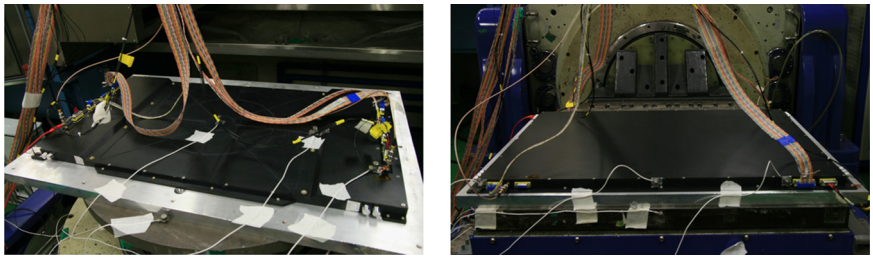

Fig. 8. TCD (left) and BCD (right) are placed on shaker for *Z*-axis and *X*-axis vibration tests.

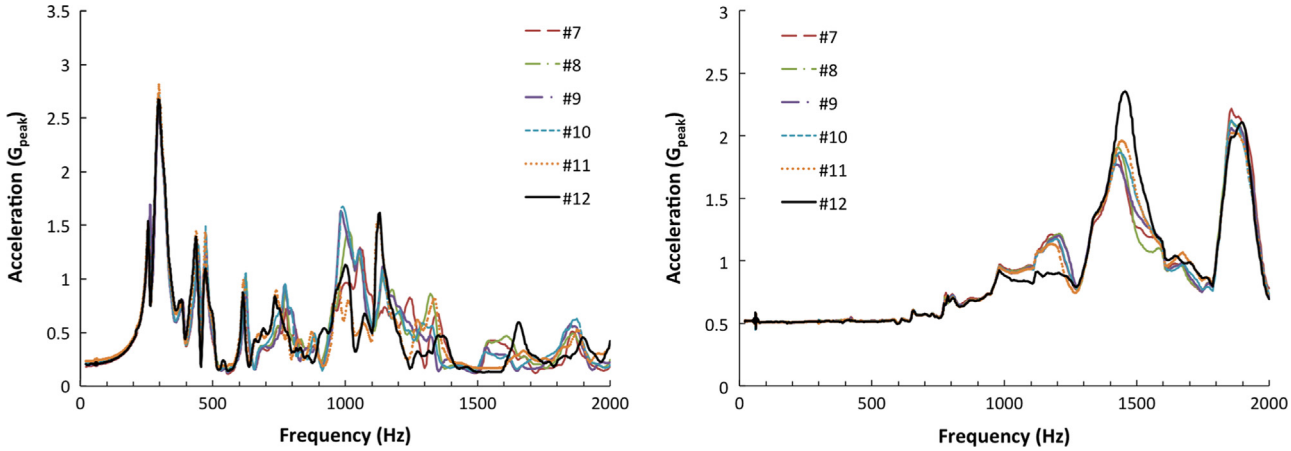

Fig. 9. Acceleration distributions as function of frequency in signature swept sine tests, which are performed between random vibration tests with different test levels. The left and right-side graphs correspond to the TCD in the *Z*-axis and the BCD in the *X*-axis, respectively.

4.2. Vibration test

A goal of the vibration test is to validate the mechanical designs and workmanship of the T/BCD by verifying its fundamental frequencies and by subjecting the detectors to levels exceeding the maximum expected levels for launch and ascent. The T/BCD are subjected to quasi-static and vibration tests in the *X*-, *Y*-, and *Z*-axes, as follows:

- Signature sine sweep: To search for resonance frequencies and establish initial conditions in the tests.
- Swept sine: To check responses of the detectors at low frequencies (5–100 Hz).
- Sine burst: To test the strength of the detectors.
- Random vibration: To study structural responses of the detectors.

The swept sine test is performed first, followed by the sine burst and random vibration tests. The signature sine sweep and functional tests are performed before and after the whole test and between each test. The frequency in the sine burst test is set to be less than one-third of detector's first resonant frequency to avoid dynamic amplification. The detailed test parameters for each item are found in Ref. [18]. During the vibration test, the detectors are carefully checked by visual inspection, and we compare the data plots of the signature sine sweep with the results of the functional tests.

Fig. 8 shows the T/BCD placed on the shaker for the *Z*- and *X*-axis vibration tests. There are four triaxial accelerometers for each T/BCD. All accelerometers are mounted by using removable adhesive, and their locations are changed depending on the axis of the vibration test. The one attached to the shaker is for controlling the shaker system, and the others are for monitoring the T/BCD's response. The control electronics are connected with the detector for the functional test and are ~1.5 m apart from the shaker. One of the test results for the signature sine sweep is indicated in Fig. 9. These data are taken from one of the accelerometers when random vibration tests with different test levels are performed for the TCD in the *Z*-axis and the BCD in the *X*-axis. Most distributions are similar in each plot except #12, which is taken after the random vibration test with the maximum test level. The maximum test level is +3 dB higher than that of the expected launch environment. This means that there is a possibility that the detectors are affected, but they exhibit normal operation in the functional test. We confirm that the detectors are not affected by the vibration test by checking and comparing the signature sine sweep with the functional test data. We also confirm by visual inspection that there are no cracks or broken parts. In the random vibration test with the maximum test level, a few connectors are loosened. Staking and stripping are performed for all connectors and screws, using an epoxy for the tightening.

5. Conclusions

Photodiodes and top and bottom counting detectors are developed for the ISS-CREAM experiment, which aims to elucidate the source and acceleration mechanisms of high-energy cosmic rays. The top and bottom counting detectors comprises 20×20 photodiode arrays coupled with plastic scintillators. The size of each photodiode is 2.3×2.3 cm^2 in the large-area photodiode array, and their electrical characteristics and various performances are investigated. The operating voltage is determined to be 200 V from the capacitance measurement, and the leakage current of each photodiode in the top and bottom counting detectors is below 20 nA/cm^2 at 200 V. The signal-to-noise ratio is measured to be better than 70 using commercial electronics, and the radiation hardness is tested using a proton beam. The test results indicate that the detectors

meet all of the requirements for physics performance. The thermal-vacuum and vibration environmental tests are performed with a flight version of the top and bottom counting detectors. The measurements indicate that the detectors can operate in harsh environments and are proven to withstand strong shocks and vibrations.

Acknowledgment

The authors thank the NASA Goddard Space Flight Center (GSFC) Wallops Flight Facility for project management and engineering support and NASA Johnson Space Center ISS Program Office for the launch support and the ISS accommodation. This work was supported in the U.S. by NASA Grant Nos. NNX11AC52G, NNX08AC15G, NNX08AC16G and their predecessor grants, as well as by directed RTOP funds to the NASA GSFC. It is supported in Korea by the Creative Research Initiatives of MEST/NRF and funded by a National Research Foundation (NRF) of Korea Grant Nos. (NRF-2014R1A1A2006456, NRF-2014R1A2A2A01002734).

References

[1] V.F. Hess, Physics Z 13 (1912) 1084.
[2] J. Beringer, J.F. Arguin, R.M. Barrett, et al., Physical Review D 86 (2012) 010001.
[3] P.L. Biermann, G. Sigl, Physics and Astrophysics of Ultra-High-Energy Cosmic Rays, Springer-Verlag, Berlin Heidelberg New York, 2001, pp 3–18.
[4] E.S. Seo, Astroparticle Physics 39/40 (2012) 76.
[5] J.R. Hörandel, Astroparticle Physics 21 (2004) 241.
[6] T. Kobayashi, Y. Komori, K. Yoshida, et al., Astrophysical Journal 601 (2004) 340.
[7] VA32HDR14.2 and TA32CG3, Gamma Medica-Ideas, Norway.
[8] Technical data sheet of EJ-200.
[9] H. Park, H.J. Hyun, D.H. Kah, et al., Journal of the Korean Physical Society 49 (2006) 1401.
[10] Electronics and Telecommunications Research Institute, Daejeon, South Korea ⟨http://www.etri.re.kr⟩.
[11] D.H. Kah, J.B. Bae, H.J. Hyun, et al., Nuclear Instruments and Methods in Physics Research Section A 628 (2011) 256.
[12] T. Ohsugi, Y. Iwata, T. Ohmoto, et al., Nuclear Instruments and Methods in Physics Research Section A 436 (1999) 272.
[13] Korea Research Institute of Standards and Science, Daejeon, South Korea ⟨http://www.kriss.re.kr⟩.
[14] Korea Institute of Radiological and Medical Sciences, Seoul, South Korea ⟨http://www.kirams.re.kr⟩.
[15] J.B. Bae, H.J. Hyun, D.H. Kah, et al., Journal of the Korean Physical Society 63 (2013) 1418.
[16] Korea Aerospace Research Institute, Daejeon, South Korea ⟨http://www.kari.re.kr⟩.
[17] The Center for Automotive Mechatronics Parts, Daegu, South Korea ⟨http://camp.kmu.ac.kr⟩.
[18] Official document of ISS-CREAM experiment, ISS-CREAM TBCD-102, CREAM T/BCD Vibration test procedure.